Efficient Water-Splitting Device Based on a Bismuth Vanadate Photoanode and Thin-Film Silicon Solar Cells

Lihao Han,*[a, d] Fatwa F. Abdi,*[b, c] Roel van de Krol,[b] Rui Liu,[d] Zhuangqun Huang,[d] Hans-Joachim Lewerenz,[d] Bernard Dam,[c] Miro Zeman,[a] and Arno H. M. Smets*[a]

A hybrid photovoltaic/photoelectrochemical (PV/PEC) water-splitting device with a benchmark solar-to-hydrogen conversion efficiency of 5.2% under simulated air mass (AM) 1.5 illumination is reported. This cell consists of a gradient-doped tungsten–bismuth vanadate (W:BiVO$_4$) photoanode and a thin-film silicon solar cell. The improvement with respect to an earlier cell that also used gradient-doped W:BiVO$_4$ has been achieved by simultaneously introducing a textured substrate to enhance light trapping in the BiVO$_4$ photoanode and further optimization of the W gradient doping profile in the photoanode. Various PV cells have been studied in combination with this BiVO$_4$ photoanode, such as an amorphous silicon (a-Si:H) single junction, an a-Si:H/a-Si:H double junction, and an a-Si:H/nanocrystalline silicon (nc-Si:H) micromorph junction. The highest conversion efficiency, which is also the record efficiency for metal oxide based water-splitting devices, is reached for a tandem system consisting of the optimized W:BiVO$_4$ photoanode and the micromorph (a-Si:H/nc-Si:H) cell. This record efficiency is attributed to the increased performance of the BiVO$_4$ photoanode, which is the limiting factor in this hybrid PEC/PV device, as well as better spectral matching between BiVO$_4$ and the nc-Si:H cell.

Introduction

Solar water splitting utilizes sunlight to produce hydrogen; a chemical fuel with the highest gravimetric energy density and a critical element for reducing carbon dioxide into useful chemical products.[1] For light-induced water splitting, transition-metal oxides, such as TiO$_2$,[2,3] WO$_3$,[4] Fe$_2$O$_3$,[5–8] and BiVO$_4$,[9,10] have been widely used as photoanode materials. In particular, BiVO$_4$ is among the most promising photoanode materials for this application because of its direct energy gap of about 2.4 eV, its environmental friendliness, and its long-term stability in neutral and basic electrolytes.[11] The theoretical solar-to-hydrogen conversion efficiency (η_{STH}) limit of this material is 9.1% with a maximum photocurrent density of 7.5 mA cm^{-2} under air mass (AM) 1.5 standard test conditions. In addition, its conduction band is located close to the hydrogen evolution potential.[12] The low carrier mobility in the material has recently been counterbalanced by introducing an internal electrical field by gradient doping with tungsten (W).[9] Carrier drift then competes favorably with the recombination processes, which results in a considerably enhanced photocurrent and makes BiVO$_4$ the photoelectrode with the hitherto highest photocurrent density within its material class.

In the taxonomy of water-splitting structures, buried junctions, as provided by photovoltaic tandem structures or metal–semiconductor Schottky barriers, are distinguished from systems in which the junction to the electrolyte determines the overall behavior. A third alternative involves structures in which part of the system's behavior is governed by the built-in rectifying junctions and, simultaneously, by the contact to the electrolyte. This type of structure is very attractive and results in devices with relatively high efficiency.[9,13–17] This is also the case for BiVO$_4$ deposited onto photovoltaic (PV) tandem solar cells, since the BiVO$_4$/electrolyte contact and the buried PV cell influence the overall behavior of the photoanode. To obtain high efficiency, it is therefore essential to optimize the performance of BiVO$_4$ and investigate various underlying tandem structures.

Herein, we improve the performance of spray-pyrolyzed BiVO$_4$ by rationalizing the design of the concentration gradient of W and simultaneously employing light-trapping techniques by depositing BiVO$_4$ onto textured fluorine-doped tin oxide (FTO) glass substrates. Although a preliminary result with a tex-

[a] L. Han,+ Prof. Dr. M. Zeman, Dr. A. H. M. Smets
Photovoltaic Materials and Devices (PVMD) Laboratory
Delft University of Technology, Mekelweg 4
2628 CD, Delft (The Netherlands)
E-mail: l.han@tudelft.nl
a.h.m.smets@tudelft.nl

[b] Dr. F. F. Abdi,+ Prof. Dr. R. van de Krol
Institute for Solar Fuels, Helmholtz-Zentrum Berlin
für Materialien und Energie GmbH
Hahn-Meitner-Platz 1, 14109 Berlin (Germany)
E-mail: fatwa.abdi@helmholtz-berlin.de

[c] Dr. F. F. Abdi,+ Prof. Dr. B. Dam
Materials for Energy Conversion and Storage (MECS) Laboratory
Delft University of Technology, Julianalaan 136
2628 BL, Delft (The Netherlands)

[d] L. Han,+ Dr. R. Liu, Dr. Z. Huang, Prof. Dr. H.-J. Lewerenz
Joint Center for Artificial Photosynthesis (JCAP)
California Institute of Technology
1200 East California Boulevard
Pasadena, CA 91125 (USA)

[+] These authors contributed equally to this work.

📖 Supporting Information for this article is available on the WWW under
http://dx.doi.org/10.1002/cssc.201402456.
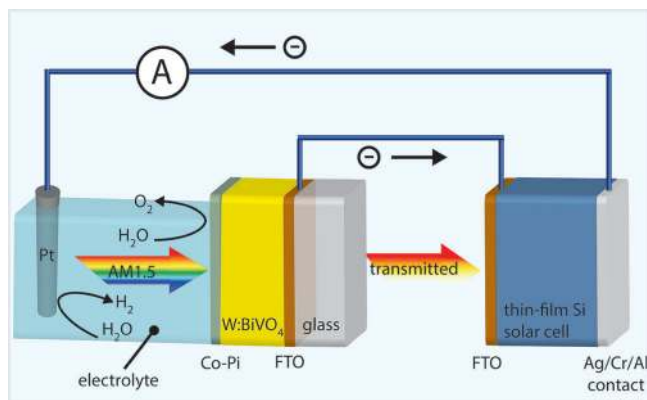
Scheme 1. Cross-sectional sketch of our PEC/PV device.

tured FTO substrate has been presented in our previous work,[9] we herein further optimize this light-trapping approach and analyze the enhancement in greater detail. This modified photoanode, when functionalized with a cobalt phosphate (Co–Pi) catalyst, provides an AM 1.5 photocurrent of 3.0 and 4.0 mA cm^{-2} at 0.75 and 1.23 V versus a reversible hydrogen electrode (RHE), respectively. Subsequently, we combined this optimized BiVO$_4$ photoanode with an amorphous silicon tandem (a-Si:H/a-Si:H) cell, a micromorph (a-Si:H/nc-Si:H) cell, and a single junction a-Si:H cell. In this tandem configuration, as shown in Scheme 1, the AM 1.5 irradiance for the rear solar cell is filtered by the front BiVO$_4$ photoanode. The current-matching conditions in the tandem (a-Si:H/a-Si:H) cell and micromorph (a-Si:H/nc-Si:H) cells are therefore sensitive to the modified shape of the solar spectrum transmitted through the photoelectrochemical (PEC) junction. The three PEC/PV tandem devices are characterized and their performance is compared herein. The tandem configuration of BiVO$_4$ and the micromorph Si solar cell has the highest solar-to-hydrogen conversion efficiency of 5.2 %, which is also the highest reported conversion efficiency for a solar water-splitting device based on metal oxides.

Results and Discussion

Absorption enhancement by light trapping in the photoanode

Light-trapping techniques have been widely investigated and applied in thin-film PV cells for decades.[18] By appropriately de-

ploying transparent conductive oxide (TCO) films with suitable root-mean-square roughness and average lateral feature size on the TCO films,[19] a relatively broad spectral range of sunlight can be scattered into large angles; hence enhancing the average absorption path length in the absorber layer. This significantly improves the absorption in the intrinsic layer and the overall performance of the PV cell. Considering the similarities to PV applications, we introduce a textured surface on the TCO substrate of a photoanode for water splitting. We compare two different FTO substrates: TEC-15 and Asahi VU-type. Figure 1 a and b provides AFM images of both substrates. The root-mean-square surface roughness of the Asahi VU-type substrate (42 nm) is much higher than that of the TEC-15 substrate (17 nm). This is better illustrated by the cross-sectional profiles of the samples shown in Figure 1 c. The textures of randomly distributed, microsized pyramid grains are adopted by the BiVO$_4$ and Co–Pi films deposited on top.

To study the potential light trapping of the substrates, two 200 nm thick BiVO$_4$ films doped with continuously decreasing concentrations of W were deposited by spray pyrolysis onto the TEC-15 (flat) and Asahi VU-type (textured) substrates. The absorption of the gradient-doped W:BiVO$_4$/FTO/glass photoanode on the flat and textured substrates is compared in Figure 1 d; this shows that light absorption is enhanced in the spectral range from $\lambda = 350$ to 490 nm in the textured sample. This textured surface affects the light management in two ways. First, the texture improves the antireflective properties of the photoanode. For photons with $\lambda < 450$ nm, the light collection efficiency is close to unity (>95 %) due to enhanced antireflection of the textured surface. Second, it enhances scattering of light into large angles, which increases its absorption
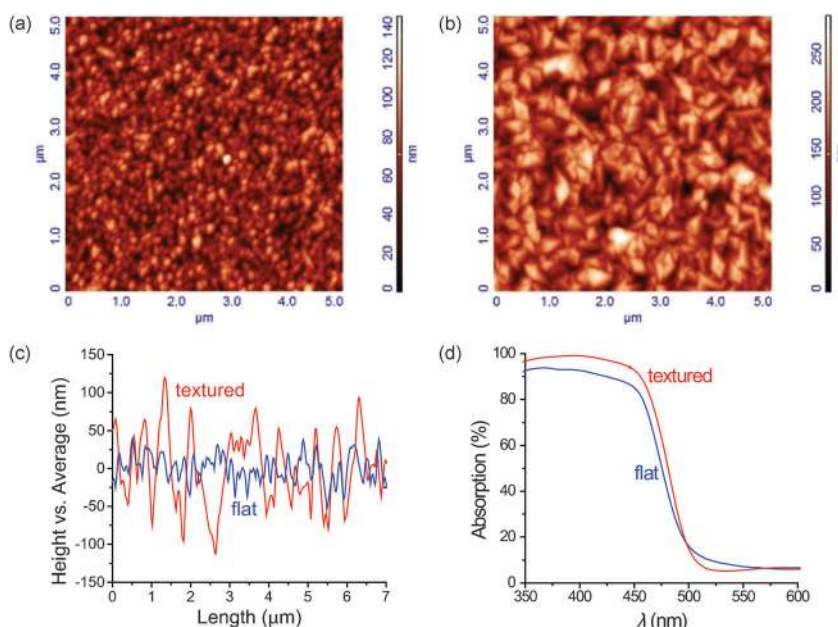

Figure 1. AFM images of (a) a flat TEC-15 FTO surface and (b) a textured Asahi VU-type FTO glass substrates; (c) the cross-sectional profile of the flat surface [from (a), blue curve] and textured substrate [from (b), red curve]. (d) Absorption of 250 nm W:BiVO$_4$ films on flat TEC-15 FTO (blue curve) and textured (Asahi VU-type) FTO-glass substrates (red curve).

path length in the BiVO$_4$ layer. This mainly affects the spectral region just above the band gap of BiVO$_4$ (450 < λ < 500 nm).

To confirm the performance improvement by the integration of textured surfaces, we compared the two-electrode current density–voltage (j–V) characteristics of the photoanode on flat and textured substrates for water splitting under AM 1.5 solar irradiance (simulated spectrum shown in Figure S1 in the Supporting Information). As shown in Figure 2, at a given voltage,
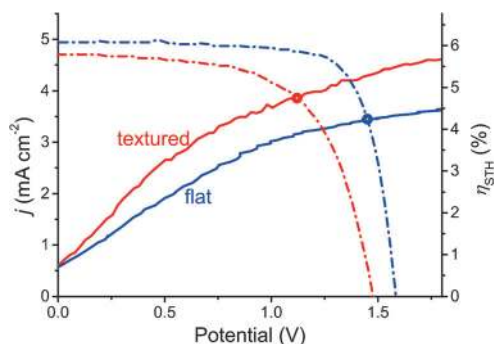

Figure 2. Light trapping in a gradient-doped Co—Pi-catalyzed W:BiVO$_4$ photoanode enhances the performance of the hybrid PEC/PV device. Solid curves are the j–V curves of the photoanodes for water splitting on flat (blue) and textured FTO substrates (red); dashed curves are the two-electrode j–V curves of the a-Si:H/a-Si:H tandem cells illuminated by AM 1.5 stimulated sunlight filtered by the corresponding photoanode. The blue and red dots are the operating points (OPs) of the a-Si:H/a-Si:H cell in combination with the flat and textured W:BiVO$_4$ photoanodes, respectively.

the current density of the photoanode on the textured substrate is generally about 25–30% higher than that of an equal thickness BiVO$_4$ film deposited on a flat substrate. This results from the improved light collection efficiency due to the textured interfaces. In addition, different textured TCO substrates, such as tin-doped indium oxide (ITO) and aluminum zinc oxide (AZO), were tested as well (data not shown herein). The use of ITO and AZO resulted in poorer performance of the photoanode than if FTO was used. We attribute this to the electrical properties of ITO and AZO being less resistant to thermal degradation under the high temperatures (450 °C) at which BiVO$_4$ is deposited and annealed.

In the hybrid PEC/PV configuration, absorption by the PEC junction at the front of the device will decrease the transmitted light available for the PV junctions at the back. Therefore, the next question that arises is how texturing of the PEC junction affects the performance of the underlying PV junctions. To study this effect, flat and textured BiVO$_4$ samples were placed in front of a previously optimized a-Si:H/a-Si:H double PV junction to act as a filter for the incident AM 1.5 light. Notably, the thickness of the a-Si:H top and bottom junctions were optimized for a flat photoanode.[17] Figure 2 shows that the open-circuit voltage (V_{OC}), short-circuit current (J_{SC}), and fill factor (FF; dashed lines in Figure 2) of the a-Si:H/a-Si:H cell are significantly lower for the textured photoanode. This is expected because the textured photoanode absorbs more light than the flat photoanode and transmits less light to the a-Si:H/a-Si:H cell. However, the operating point (OP) of the textured device, which is

given by the intersection of the PEC and PV j–V curves,[9,14–15,17] is at a higher photocurrent density than that of the flat device. In a working hybrid device in which the PEC and PV junctions are connected in series, η_{STH} is determined from Equation (1):

$$\eta_{STH} = \frac{J_{OP} \times 1.23 \text{ V}}{100 \text{ V cm}^{-2}} \qquad (1)$$

in which J_{OP} is operating photocurrent density of the system in mA cm^{-2} and the value of 1.23 V is the thermodynamic potential for water splitting [H$_2$O(l)→H$_2$(g)+O$_2$(g)]. The value of 100 mW cm^{-2} corresponds to the total power density of AM 1.5 sunlight. It is clear from Equation (1) that η_{STH} is only determined by the photocurrent density at the OP (assuming 100% Faradaic efficiency). Therefore, despite the poorer j–V characteristics of the a-Si:H/a-Si:H cell when placed behind the textured photoanode, the textured device does give a higher value of η_{STH}. Specifically, the intersection point of the j–V curve of the photoanode on the textured substrate (red hollow dot in Figure 2) shows that light trapping in the photoanode enhances the η_{STH} by about 12% compared with the photoanode on the flat substrate (blue hollow dot in Figure 2).

Doping profile optimization on the photoanode

Because the optical absorption in BiVO$_4$ plays an important role in improving the η_{STH} value of the resulting device, we also studied the effect of increasing the thickness of the BiVO$_4$ film. Initially, we prepared 250 and 300 nm thick BiVO$_4$ films, each with the same 10-step gradient in W dopant concentration. This means that the thickness of each step is 25 and 30 nm for the 250 and 300 nm thick films, respectively. Although these two films clearly absorb more light than the 200 nm thick film with the same 10-step gradient doping, the resulting photocurrents decrease (data not shown). We believe that the reason for this decrease is related to the competing effects of enhanced light absorption and poorer carrier collection efficiency (η_{col}, sometimes also referred as carrier separation efficiency, η_{sep}) in thicker films.[20] The performance decrease indicates that the detrimental influence on carrier collection efficiency apparently outweighs the improvement in light absorption upon increasing the film thickness from 250 to 300 nm.

Recently, we reported a time-resolved microwave conductivity study on spray-pyrolyzed BiVO$_4$ films.[21] The carrier diffusion length in undoped BiVO$_4$ was about 70 nm. Mobility measurements on a BiVO$_4$ single crystal revealed a comparable carrier diffusion length.[22] This means that carriers (electrons and holes) can travel about 70 nm by diffusion in undoped BiVO$_4$ before they eventually recombine. Taking this into account, we prepared a 250 nm thick gradient-doped W:BiVO$_4$ film with a different gradient profile. The thickness of the layer for each dopant step was kept at 20 nm, except for the last step (undoped layer), which was 70 nm. This allowed us to increase the thickness of an optimized 200 nm thick gradient-doped film to 250 nm, without affecting the carrier collection efficiency (Figure 3a and b). Figure 3c shows that the AM 1.5 photocurrent
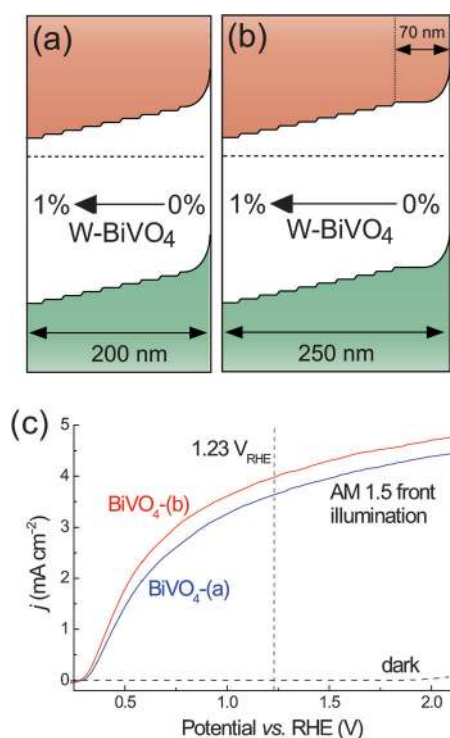
Figure 3. Schematic illustration of the band diagram of the 200 nm reference gradient-doped W:BiVO$_4$ sample (a) and the 250 nm modified gradient-doped W:BiVO$_4$ sample (b). The electrolyte is on the right-hand side and the FTO substrate is on the left. (c) Three-electrode AM 1.5 photocurrent density versus potential (*j–V*) curves of the samples depicted in a) and b) under front illumination (light enters through the electrolyte). Both samples are catalyzed with Co−Pi. The dashed curve (black line) shows the dark current density of the samples.

density indeed increases after this modification. AM 1.5 photocurrent densities as high as 3 and 4 mA cm^{-2} are achieved at potentials of 0.75 and 1.23 V versus RHE, respectively, with excellent reproducibility (Figure S2 in the Supporting Information). This is a 10–15 % improvement relative to the 200 nm thick gradient-doped W:BiVO$_4$ reported by us previously,[9] and comparable to the photocurrent densities recently reported by Choi and Kim for their nanostructured BiVO$_4$–FeOOH–NiOOH system.[23] The observed improvement illustrates the significance of the rational design of the dopant profile in a metal oxide photoanode for water splitting.

Spectral matching in the PEC/PV configuration

We demonstrated in our previous report that the profiles of the external quantum efficiency (EQE) spectra for the thin-film silicon cells in a tandem PEC/PV configuration (Scheme 1) were highly sensitive to the presence of a front anode structure.[17] Considering the improvements for the BiVO$_4$ front photoanode, further optimization of the rear silicon cell needs to be done, and higher η_{STH} may be expected. The dependence of the rear cell to the front photoanode mainly results because the same current has to flow through all (series-connected) components in the PEC/PV tandem device and significant spectral overlap between the absorption of BiVO$_4$ and a-Si:H

used. This current-matching requirement suggests that further improvements can be made by extending the spectral utilization of the bottom PV cell. Therefore, we expect a higher value of η_{STH} through the introduction of a micromorph silicon solar cell. The spectral utilization of the nc-Si:H bottom cell is extended to the near-infrared (NIR) range ($\lambda < 1100$ nm; Figure 4), further than the a-Si:H bottom cell ($\lambda < 800$ nm) in the previously used a-Si:H/a-Si:H tandem cell.
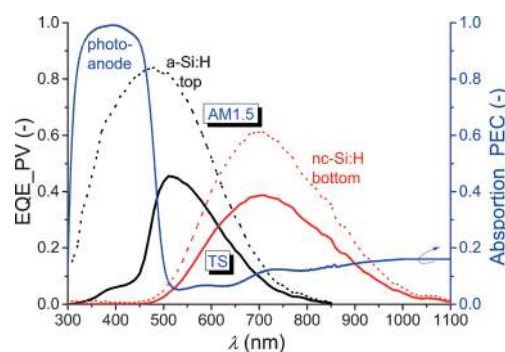

Figure 4. The EQE curves of the a-Si:H/nc-Si:H solar cell, the a-Si:H top junction (black), and the nc-Si:H bottom junction (red). Dashed curves indicate EQE spectra of the PV junctions under full AM 1.5 simulated solar illumination; solid curves indicate the EQE spectra measured with a Co−Pi-coated BiVO$_4$ photoanode placed in front of the solar cells. The blue curve represents the optical absorption spectrum of the Co−Pi-coated BiVO$_4$ photoanode.

For this new PEC/PV device, the spectral response of each component illuminated by standard AM 1.5 irradiance was measured, as shown by the solid curves in Figure 4. The dashed curves represent the *j–V* curves of the PV cells without the Co−Pi-catalyzed BiVO$_4$ photoanode in the front. Because of the spectral overlap of the photoanode (Figure 4, solid blue line) and the a-Si:H PV junction, the EQE of the a-Si:H is reduced by a factor of about 10 below $\lambda = 450$ nm. In contrast, the absorption in the nc-Si:H layer is less affected by the absorption in BiVO$_4$—the reduction of its EQE is primarily caused by reflection and scattering losses—and the shape of the spectral response is relatively unchanged. The reflection losses can be further minimized by optimizing the refractive indices of the front layers, which is beyond the scope of this work. Integrating the modified EQE of the micromorph silicon solar cell allows us to predict the short-circuit photocurrent density of the cell, which is 5.91 mA cm^{-2} (top a-Si:H cell limited). This value is higher than that of the a-Si:H/a-Si:H cell (4.37 mA cm^{-2}), and provides additional room for the improved performance of our BiVO$_4$.

In addition to the spectral match requirement, the *j–V* characteristics of the PV cell should match those of the PEC cell to optimize the performance. The *j–V* characteristics of the latter are mostly determined by the optical absorption, the carrier collection efficiency, and the catalytic efficiency of the semiconductor photoanode.[24] The two-electrode *j–V* characteristics of various thin-film silicon PV cells and the Co−Pi-catalyzed 250 nm thick gradient-doped W:BiVO$_4$ photoanode are shown

in Figure 5. The operating current density, voltage, and the η_{STH} values of the various PEC/PV combinations are listed in Table 1, together with the performance parameters of the respective PV cells (η_{PV} is the conversion efficiency of the standalone PV junctions illuminated by the specific spectrum). Figure 5a shows that the operating photocurrent densities of W:BiVO$_4$/a-Si:H/a-Si:H and W:BiVO$_4$/micromorph (a-Si:H/nc-Si:H) are similar, despite the differences in the characteristics of the PV components. A closer look, however, reveals that the operating photocurrent density of the W:BiVO$_4$/micromorph Si is slightly higher, just above 4.22 mA cm^{-2} (Figure 5b). This higher photocurrent density is due to smaller spectral overlap between the

micromorph Si and BiVO$_4$, compared with the overlap between the a-Si:H/a-Si:H and BiVO$_4$.

Short-circuit photocurrent density measurements of the PEC/PV device confirm the operating photocurrent predicted by the intersection of the j–V curves (Figure S3 in the Supporting Information). The photocurrent is also relatively stable within the course of an hour, with less than 5% degradation observed. Multiple reports with the same material system (W-doped BiVO$_4$ and Co–Pi) have confirmed that the Faradaic efficiency is effectively 100%.[25] By taking this into account, the 4.22 mA cm^{-2} photocurrent density that we observe with the combination of BiVO$_4$ and micromorph Si corresponds to an apparent η_{STH} of 5.2%, which represents the current benchmark for standalone water-splitting devices based on a metal oxide photoelectrode.[9–10,26]

Although the increase in η_{STH} (4.9[9] to 5.2%) may seem incremental, the implication is very significant. Recent technoeconomic analyses have shown that efficiency is the most important knob in determining the resulting cost of hydrogen.[27,28] This is of course unsurprising, as also demonstrated in the solar cells field.

Figure 5 also shows that the combination of an optimized W:BiVO$_4$ photoanode and an optimized single-junction a-Si:H can result in a relatively high η_{STH} of 4.6%. This is only about 11% lower than the record efficiency we report herein, but using fewer layers (p-i-n + buffer layers). This means that the processing time and costs of the device are significantly reduced. Moreover, the results in Figure 5a clearly show that the BiVO$_4$ photocurrent density at around 0.8–0.9 V limits the overall performance of the device. With a theoretical photocurrent density of 7.5 mA cm^{-2} for BiVO$_4$, there is plenty of room for improvement by the combination of BiVO$_4$ and single-junction a-Si:H. In contrast, only little improvements are possible for the BiVO$_4$/double-junction Si cell devices, in which the total photocurrent density is already close to the maximum photocurrent density of the double-junction Si cell.[9,10,17] A configuration with a single-junction a-Si:H cell therefore seems the most promising route for the further development of hybrid PEC/PV devices.

Finally, it is imperative that the platinum counter electrode used herein for convenience needs to be replaced by an earth-abundant alternative. For example, one may consider various earth-abundant hydrogen evolution catalysts, such as the transition-metal alloys (NiMo, NiMoZn,[26] NiFeMo, CoMo[29]), metal sulfides (MoS$_2$,[30,31] WS$_2$[32]), and the newly emerged metal phosphides (Co$_2$P, Ni$_2$P[33]). These materials are already highly developed and demonstrate high activities at relatively low overpotentials.

Figure 5. (a) Matching of the two-electrode j–V curves between PV cells and the photoanode, which indicates that the micromorph Si cell can beat the a-Si:H/a-Si:H device when the performance of the photoanode is improved. A η_{STH} of 5.2% record is achieved. The j–V curves of the PV cells are measured by using AM 1.5 illumination filtered with the Co–Pi-catalyzed, 250 nm thick gradient-doped W:BiVO$_4$ photoanode. (b) Magnification of the central part of (a).

Conclusions

A new benchmark of 5.2% solar-to-hydrogen conversion efficiency of a metal oxide based device has been obtained by optimizing the absorption and carrier collection in a BiVO$_4$ photoanode, and combining it with a micromorph Si tandem cell to form a standalone hybrid PEC/PV tandem device. The increased absorption is obtained through the employment of
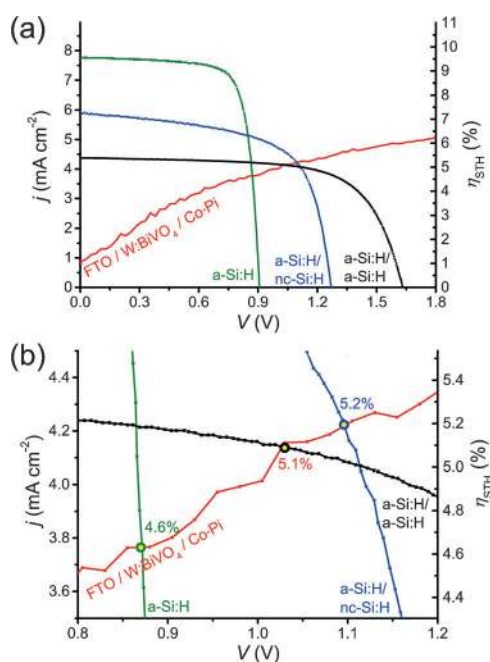
Table 1. External parameters of three thin-film silicon solar cells and the hybrid PEC/PV device when each of them is combined with the Co–Pi catalyzed, 250 nm thick gradient-doped W:BiVO$_4$ photoanode.

Conditions	PV parameters	a-Si:H	a-Si:H/a-Si:H	a-Si:H/nc-Si:H
AM 1.5 illumination	V_{OC} [V]	0.93	1.68	1.32
	J_{SC} [mA cm^{-2}]	13.92	6.18	11.63
	FF [%]	76.3	69.8	62.4
	η_{PV} [%]	9.9	7.3	9.6
photoanode-filtered AM 1.5 illumination	V_{OC} [V]	0.91	1.63	1.27
	J_{SC} [mA cm^{-2}]	7.76	4.37	5.91
	FF [%]	76.9	67.8	63.5
	η_{PV} [%]	5.4	4.8	4.8
OP	V_{OP} [V]	0.87	1.03	1.10
	J_{OP} [mA cm^{-2}]	3.77	4.14	4.22
	η_{STH} [%]	4.6	5.1	5.2

textured substrates and by increasing the film thickness, while retaining a high carrier collection efficiency by rational design of the gradient W-dopant concentration profile in BiVO$_4$. The combination with a micromorph silicon cell allows better utilization of the AM 1.5 solar spectrum, compared with the earlier demonstration of a tandem system with a-Si:H/a-Si:H cell, due to the extended absorption of the nc-Si:H bottom junction up to about 1100 nm. Further improvement of the performance of the BiVO$_4$ photoanode may be possible through nanostructuring and/or by employing metal plasmonic nanoparticles to improve the light absorption closed to the band edge. When these photoanodes reach photocurrent densities in excess of about 5 mA cm^{-2}, the use of a single-junction a-Si:H cell may lead to higher efficiencies than double-junction a-Si:H-based PV cells. As such, the combination of chemically stable metal oxide absorbers with efficient silicon-based PV devices offers a realistic pathway towards efficient, simple, solar water-splitting devices from earth-abundant elements.

Experimental Section

Thin-film silicon solar cells were deposited by a radio frequency plasma-enhanced chemical vapor deposition (RF-PECVD) multi-chamber tool. The 2.5 cm × 10 cm Asahi VU-type substrate (≈600 nm thick textured FTO layer on glass) was heated at 170 °C during the Si thin-film deposition.

The p layers in the a-Si:H cell and a-Si:H/a-Si:H cell are based on a-SiC:H(B), the i layers are based on a-Si:H, and the n layers are phosphorus-doped nanocrystalline silicon oxide [nc-SiO$_x$:H(P)]. The thickness of the i layer of single-junction a-Si:H cell was 300 nm. The thicknesses of the i layers in the a-Si:H/a-Si:H double junction were 100 and 350 nm for the top and bottom junctions, respectively, and were optimized according to our previous work.[17] In the micromorph Si solar cell, the p layers were based on nc-SiO$_x$:H(B), and the thicknesses of the i layers were 300 nm for a-Si:H and 1800 nm for nc-Si:H. After the Si thin films were synthesized, a stripe of 300 nm Al was coated by rotating Provac evaporator on the precovered region of the sample as the front contact. Each metal back contact had an area of 1 cm × 1 cm. The structure sketches of the three PV cells are illustrated in Schemes S1–S3 in the Supporting Information.

Gradient-doped W:BiVO$_4$ with a thickness of 200 nm was synthesized by spray pyrolysis, as reported previously.[17] In the 250 nm thick gradient-doped W:BiVO$_4$, 50 additional spray cycles of the undoped BiVO$_4$ precursor solution were performed. Two types of TCO-coated glass substrates were used in spray pyrolysis. One was TEC-15 F:doped SnO$_2$ (FTO) glass (Hartford Glass Co.), which had a relatively flat surface; and the other was an Asahi VU-type substrate (Asahi Glass Co.), which was an FTO-coated glass with random sharp features as the texturing layer. Electrical contacts to the BiVO$_4$ photoanode in the tandem devices were established by using silver wire and graphite paste. Co—Pi catalyst was electrodeposited on the surface of BiVO$_4$ according to previous reports.[26]

Three-electrode PEC performance was measured in a 0.1 M aqueous solution of KPi (pH≈7) with a platinum wire and a Ag/AgCl electrode (XR300, saturated KCl and AgCl solution, Radiometer Analytical) as the counter and reference electrodes, respectively. Two-electrode PEC performance was measured in the same electrolyte with the samples as the working electrode and platinum wire as the counter electrode. Simulated AM 1.5 solar illumination (100 mW cm^{-2}) was achieved with a Newport Sol3A Class AAA solar simulator (94023A-SR3 type) as the light source. In all PEC measurements, a circular area with a diameter of 6 mm on each sample was illuminated, which corresponded to a total area of 0.283 cm^2. The current density–potential profiles of the working electrode were monitored by means of a potentiostat (EG&G PAR 283).

[1] M. G. Walter, E. L. Warren, J. R. McKone, S. W. Boettcher, Q. X. Mi, E. A. Santori, N. S. Lewis, *Chem. Rev.* **2010**, *110*, 6446–6473.
[2] A. Fujishima, K. Honda, *Nature* **1972**, *238*, 37.
[3] S. U. M. Khan, M. Al-Shahry, W. B. Ingler, *Science* **2002**, *297*, 2243–2245.
[4] R. Liu, Y. Lin, L. Y. Chou, S. W. Sheehan, W. He, F. Zhang, H. J. Hou, D. Wang, *Angew. Chem. Int. Ed.* **2011**, *50*, 499–502; *Angew. Chem.* **2011**, *123*, 519–522.
[5] I. Cesar, A. Kay, J. A. Gonzalez Martinez, M. Grätzel, *J. Am. Chem. Soc.* **2006**, *128*, 4582–4583.
[6] L. Y. Chou, R. Liu, W. S. He, N. Geh, Y. J. Lin, E. Y. F. Hou, D. W. Wang, H. J. M. Hou, *Int. J. Hydrogen Energy* **2012**, *37*, 8889–8896.
[7] Y. Ling, G. Wang, J. Reddy, C. Wang, J. Z. Zhang, Y. Li, *Angew. Chem. Int. Ed.* **2012**, *51*, 4074–4079; *Angew. Chem.* **2012**, *124*, 4150–4155.
[8] X. Yang, C. Du, R. Liu, J. Xie, D. Wang, *J. Catal.* **2013**, *304*, 86–91.
[9] F. F. Abdi, L. Han, A. H. M. Smets, M. Zeman, B. Dam, R. van de Krol, *Nat. Commun.* **2013**, *4*, 2195.
[10] M. F. Lichterman, M. R. Shaner, S. G. Handler, B. S. Brunschwig, H. B. Gray, N. S. Lewis, J. M. Spurgeon, *J. Phys. Chem. Lett.* **2013**, *4*, 4188–4191.
[11] F. F. Abdi, N. Firet, A. Dabirian, R. van de Krol, *MRS Proceedings* **2012**, *1446*, mrss12-1446-u02-05, DOI: 10.1557/opl.2012.811.
[12] S. J. Hong, S. Lee, J. S. Jang, J. S. Lee, *Energy Environ. Sci.* **2011**, *4*, 1781–1787.
[13] O. Khaselev, J. A. Turner, *Science* **1998**, *280*, 425–427.
[14] E. L. Miller, B. Marsen, D. Paluselli, R. Rocheleau, *Electrochem. Solid-State Lett.* **2005**, *8*, A247–A249.
[15] N. Gaillard, Y. Chang, J. Kaneshiro, A. Deangelis, E. L. Miller, *Proc. Soc. Photo-Opt. Instrum.* **2010**, *7770*, 77700V.
[16] J. Brillet, J. H. Yum, M. Cornuz, T. Hisatomi, R. Solarska, J. Augustynski, M. Grätzel, K. Sivula, *Nat. Photonics* **2012**, *6*, 824–828.
[17] L. Han, F. F. Abdi, P. Perez Rodriguez, B. Dam, R. van de Krol, M. Zeman, A. H. M. Smets, *Phys. Chem. Chem. Phys.* **2014**, *16*, 4220–4229.
[18] K. Jäger, O. Isabella, L. Zhao, M. Zeman, *Phys. Status Solidi C* **2010**, *7*, 945–948.
[19] C. Battaglia, C. M. Hsu, K. Söderström, J. Escarre, F. J. Haug, M. Charriere, M. Boccard, M. Despeisse, D. T. L. Alexander, M. Cantoni, Y. Cui, C. Ballif, *ACS Nano* **2012**, *6*, 2790–2797.
[20] F. F. Abdi, N. Firet, R. van de Krol, *ChemCatChem* **2013**, *5*, 490–496.
[21] F. F. Abdi, T. J. Savenije, M. M. May, B. Dam, R. van de Krol, *J. Phys. Chem. Lett.* **2013**, *4*, 2752–2757.
[22] A. J. E. Rettie, H. C. Lee, L. G. Marshall, J. F. Lin, C. Capan, J. Lindemuth, J. S. McCloy, J. S. Zhou, A. J. Bard, C. B. Mullins, *J. Am. Chem. Soc.* **2013**, *135*, 11389–11396.
[23] T. W. Kim, K.-S. Choi, *Science* **2014**, *343*, 990–994.
[24] H. Dotan, K. Sivula, M. Grätzel, A. Rothschild, S. C. Warren, *Energy Environ. Sci.* **2011**, *4*, 958–964.

[25] D. K. Zhong, S. Choi, D. R. Gamelin, *J. Am. Chem. Soc.* **2011**, *133*, 18370–18377.

[26] S. Y. Reece, J. A. Hamel, K. Sung, T. D. Jarvi, A. J. Esswein, J. J. H. Pijpers, D. G. Nocera, *Science* **2011**, *334*, 645–648.

[27] G. N. B. B. D. James, J. Perez, K. N. Baum, in Directed Technologies Inc., *Department of Energy contract GS-10F-009J Technical Report*, **2009**, pp. 1–127.

[28] B. A. Pinaud, J. D. Benck, L. C. Seitz, A. J. Forman, Z. B. Chen, T. G. Deutsch, B. D. James, K. N. Baum, G. N. Baum, S. Ardo, H. L. Wang, E. Miller, T. F. Jaramillo, *Energy Environ. Sci.* **2013**, *6*, 1983–2002.

[29] A. W. Jeremiasse, J. Bergsma, J. M. Kleijn, M. Saakes, C. J. N. Buisman, M. C. Stuart, H. V. M. Hamelers, *Int. J. Hydrogen Energy* **2011**, *36*, 10482–10489.

[30] T. F. Jaramillo, K. P. Jørgensen, J. Bonde, J. H. Nielsen, S. Horch, I. Chorkendorff, *Science* **2007**, *317*, 100–102.

[31] J. Kibsgaard, Z. B. Chen, B. N. Reinecke, T. F. Jaramillo, *Nat. Mater.* **2012**, *11*, 963–969.

[32] D. Voiry, H. Yamaguchi, J. W. Li, R. Silva, D. C. B. Alves, T. Fujita, M. W. Chen, T. Asefa, V. B. Shenoy, G. Eda, M. Chhowalla, *Nat. Mater.* **2013**, *12*, 850–855.

[33] E. J. Popczun, J. R. McKone, C. G. Read, A. J. Biacchi, A. M. Wiltrout, N. S. Lewis, R. E. Schaak, *J. Am. Chem. Soc.* **2013**, *135*, 9267–9270.